Tuning Nucleation Kinetics via Nonequilibrium Chemical Reactions

Yongick Cho and William M. Jacobs

Phys. Rev. Lett. **130**, 128203 — Published 24 March 2023

DOI: 10.1103/PhysRevLett.130.128203

Tuning nucleation kinetics via nonequilibrium chemical reactions

Yongick Cho[1] and William M. Jacobs[1, *]
[1] *Department of Chemistry, Princeton University, Princeton, New Jersey 08544, USA*

(Dated: February 23, 2023)

Unlike fluids at thermal equilibrium, biomolecular mixtures in living systems can sustain nonequilibrium steady states, in which active processes modify the conformational states of the constituent molecules. Despite qualitative similarities between liquid–liquid phase separation in these systems, the extent to which the phase-separation kinetics differ remains unclear. Here we show that inhomogeneous chemical reactions can alter the nucleation kinetics of liquid–liquid phase separation in a manner that is consistent with classical nucleation theory, but can only be rationalized by introducing a nonequilibrium interfacial tension. We identify conditions under which nucleation can be accelerated without changing the energetics or supersaturation, thus breaking the correlation between fast nucleation and strong driving forces that is typical of phase separation and self-assembly at thermal equilibrium.

In living systems, phase separation can occur at a nonequilibrium steady state (NESS) as opposed to thermal equilibrium [1, 2]. For example, in active intracellular condensates, biomolecules may be degraded or post-translationally modified by enzymes that couple conformational changes to the conversion of a chemical fuel, such as ATP, to chemical waste [3]. Although chemically driven fluids can undergo phase transitions resembling those of equilibrium systems, the phase behavior can be much richer when the enzymes that drive the reactions preferentially localize to one phase or when chemical fuel gradients couple to the local density of the phase-separating molecules [4–6]. For example, phase separation taking place at a NESS can exhibit qualitatively different features compared to thermal equilibrium, including suppressed coarsening, monodisperse phase-separated droplet size distributions, and even spontaneous droplet division [7–10].

Driven chemical reactions can also affect the kinetics of phase transitions, although the extent to which kinetic pathways at a NESS differ from those at equilibrium is not well understood. Not only do driven chemical reactions provide additional control parameters beyond temperature and concentration with which to control a phase transition, but they might also alter the mechanism of phase separation. This possibility contrasts with the behavior of equilibrium phase-separating fluids, in which strong thermodynamic driving forces are typically necessary to initiate homogeneous nucleation at equilibrium unless the system is near a critical point [11, 12]. The consequences of this correlation between thermodynamics and nucleation kinetics are well appreciated in the context of molecular self-assembly, especially in cases where strong driving forces are associated with kinetic trapping [13–17]. In principle, living systems must contend with similar trade-offs in order to harness phase separation for biological functionality [18, 19].

Here we show that driven chemical reactions provide a mechanism to alter the nucleation pathway of a nonequilibrium phase-separating fluid. To build intuition, we first describe simulations of phase coexistence and nucleation in a model of a fluid with driven chemical reactions, and we identify the conditions under which nucleation at a NESS cannot be described by an equilibrium theory. Then, by introducing a general theoretical framework, we show that the difference between equilibrium and nonequilibrium nucleation kinetics arises from a nonequilibrium interfacial tension between the phases. Our theoretical results establish how emergent interfacial properties can tune the kinetics of phase separation and self-assembly far from equilibrium.

In order to study nonequilibrium phase separation via molecular simulation, we adopt the framework of stochastic thermodynamics [20, 21] and consider an open system connected to a particle reservoir (Fig. 1a). For simplicity, we perform simulations using a two-dimensional square lattice model, in which empty lattice sites represent solvent. We assume that the particles have two internal states: a bonding state (B) that promotes phase separation due to attractive nearest neighbor interactions with bond energy $\epsilon < 0$, and an inert state (I) that is isoenergetic to an empty lattice site. The internal free-energy difference between the internal states in the reservoir is Δf_{res}, so that the fugacities of the two states are related by $z_{\text{B}}/z_{\text{I}} = \exp(-\beta\Delta f_{\text{res}})$, where $\beta \equiv (k_{\text{B}}T)^{-1}$. Our model is closely related to the equilibrium lattice gas, which exhibits a first-order phase transition between a dilute vapor (v) phase and a condensed liquid (l) phase below a critical temperature [22]. However, unlike the equilibrium lattice gas, particle transitions between the system and the reservoir in our model may not obey time-reversal symmetry. The product of rates for inserting a bonding particle, changing its internal state, and returning it to the reservoir may therefore differ from that of the reversed sequence by a factor $\exp(\beta\Delta\mu)$, where $\Delta\mu$ is the chemical potential difference used to drive reactions between the internal states inside the system (Appendix A). We assume that $\Delta\mu$ is uniform throughout the system.

Interconversion between B and I states can occur either directly or via exchange with the reservoir. The ratio of

---

[*] wjacobs@princeton.edu

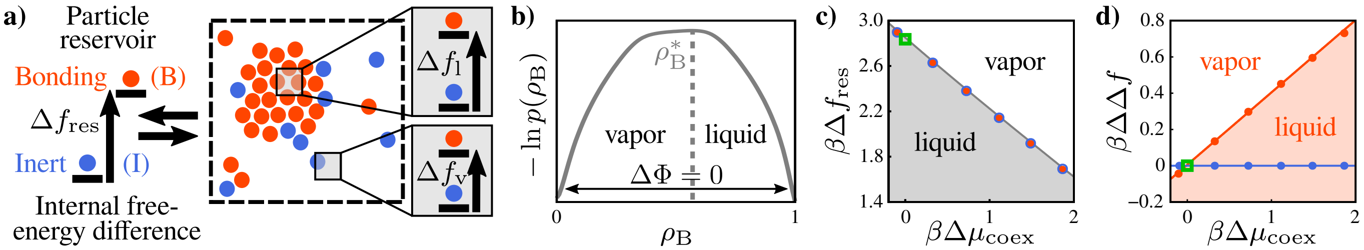

FIG. 1. **Simulating driven chemical reactions at a phase-separated NESS. (a)** Schematic of an open system with inhomogeneous chemical reactions. The effective internal free-energy differences between the B and I states in the liquid and vapor phases are Δf_{l} and Δf_{v}, respectively. **(b)** An example steady-state distribution in an inhomogeneous model. **(c)** Phase diagram for equilibrium (green), nonequilibrium homogeneous (blue), and inhomogeneous (orange) models, and **(d)** quantification of the inhomogeneous reactions assuming $\beta\epsilon = -2.95$, $k^\circ = 10^{-1}$, and $\rho_{\mathrm{v}} = 0.05$ at coexistence. The shaded (unshaded) region indicates where liquid (vapor) is stable for all models in (c) and for the inhomogeneous model only in (d).

the direct forward and backward B $\rightleftharpoons$ I reaction rates is controlled by $\Delta\mu$ in accordance with "local detailed balance" [20, 21]. Meanwhile, the reservoir-mediated pathway is governed by Δf_{res}. The steady-state populations are therefore influenced by the relative fluxes through these competing pathways, which can be tuned by specifying the rate for I → B transitions, $k_{\mathrm{I}\to\mathrm{B}}$. If $k_{\mathrm{I}\to\mathrm{B}}$ is constant, then the chemical reactions are *homogeneous*. By contrast, if $k_{\mathrm{I}\to\mathrm{B}}$ is influenced by the local environment, then we refer to the reactions as *inhomogeneous*. In our lattice model, fluids with inhomogeneous chemical reactions have a $k_{\mathrm{I}\to\mathrm{B}}$ rate that depends on the nearest-neighbor particles and thus on the local potential energy.

To quantify inhomogeneous chemical reactions at a NESS, we introduce an *effective* internal free-energy difference, $\beta\Delta f \equiv -\ln(\rho_{\mathrm{B}}/\rho_{\mathrm{I}}) + \ln\langle\exp(-\beta\Delta u_{\mathrm{I}\to\mathrm{B}})\rangle_{\mathrm{I}}$, where ρ_{B} and ρ_{I} are the steady-state number densities of particles in the B and I states, respectively, and the second term represents an average of the potential energy change due to converting an I to a B particle at steady state (Appendix A). At equilibrium, $\Delta f = \Delta f_{\mathrm{res}}$. At a NESS, an explicit dependence of $k_{\mathrm{I}\to\mathrm{B}}$ on the local potential energy causes Δf to differ between the liquid and the vapor phases, such that $\Delta\Delta f \equiv \Delta f_{\mathrm{l}} - \Delta f_{\mathrm{v}} \neq 0$. Although this mapping between nonequilibrium and equilibrium models is not exact in general, measuring $\Delta\Delta f$ provides crucial insight into the differences between fluids with inhomogeneous and homogeneous reactions.

We illustrate the differences between homogeneous and inhomogeneous chemical reactions by performing kinetic Monte Carlo simulations [23] of a particular nonequilibrium fluid model. We consider a fluid in which $\Delta f_{\mathrm{res}} > 0$, meaning that the I state is more populous in the vapor phase, while bonding stabilizes the B state in the liquid phase (Fig. 1a). We implement chemical reactions by assuming Markovian transitions and local detailed balance, such that reactions taking place inside the system are controlled by $\Delta\mu$ (Appendix A). We obtain homogeneous reactions if we set $k_{\mathrm{I}\to\mathrm{B}}$ equal to a constant, k°, which represents the ratio between the timescales for internal state changes and particle diffusion. To obtain inhomogeneous reactions, we assume that the I → B transition rate is a decreasing function of the local potential energy, u, at a lattice site (Appendix A). We emphasize that due to local detailed balance, this choice of $k_{\mathrm{I}\to\mathrm{B}}$ implies that *both* the I → B and B → I rates are enhanced at low potential energy when positive chemical drive is applied, resulting in an increased Δf in the liquid relative to the vapor phase (Fig. 1a).

We identify the conditions for nonequilibrium phase coexistence with both homogeneous and inhomogeneous reactions by equating the total probability of being in the vapor versus the liquid phase at steady state (Fig. 1b). This is analogous to the equal pressure construction in equilibrium grand-canonical phase-coexistence simulations [24], and implies that the open system transitions between the liquid and vapor phases with equal forward and backward rates. To this end, we use a form of nonequilibrium umbrella sampling [25] to calculate the steady-state probability as a function of the number density of bonding particles, $p(\rho_{\mathrm{B}})$ [26]. As is characteristic of a first-order phase transition, we observe a barrier with respect to $-\ln p(\rho_{\mathrm{B}})$ that scales with the lattice length L as the system size is increased [27]. Based on the value of the order parameter ρ_{B}^* at the top of this barrier, we determine the steady-state probabilities of the vapor and liquid phases, $p_{\mathrm{v}} \equiv \int_0^{\rho_{\mathrm{B}^*}} p(\rho_{\mathrm{B}})d\rho_{\mathrm{B}}$ and $p_{\mathrm{l}} \equiv \int_{\rho_{\mathrm{B}^*}}^1 p(\rho_{\mathrm{B}})d\rho_{\mathrm{B}}$, respectively. We then define the dimensionless thermodynamic driving force between bulk phases to be $\beta\Delta\Phi \equiv L^{-2}\ln(p_{\mathrm{l}}/p_{\mathrm{v}})$ and associate phase coexistence with $\Delta\Phi = 0$ (Fig. 1c). As anticipated, measuring $\Delta\Delta f$ between coexisting phases confirms that only the potential-energy dependent choice for $k_{\mathrm{I}\to\mathrm{B}}$ results in inhomogeneous reactions, regardless of $\Delta\mu_{\mathrm{coex}}$, the nonequilibrium drive at coexistence (Fig. 1d).

We can now address the central question of this work: To what extent can equilibrium descriptions of nucleation be applied to phase separation at a NESS? The most widely used theoretical framework for describing nucleation in systems ranging from atomic and molecular fluids to colloidal and biomolecular materials is classical nucleation theory (CNT) [11, 12]. In its most general form, equilibrium CNT predicts that nucleation follows

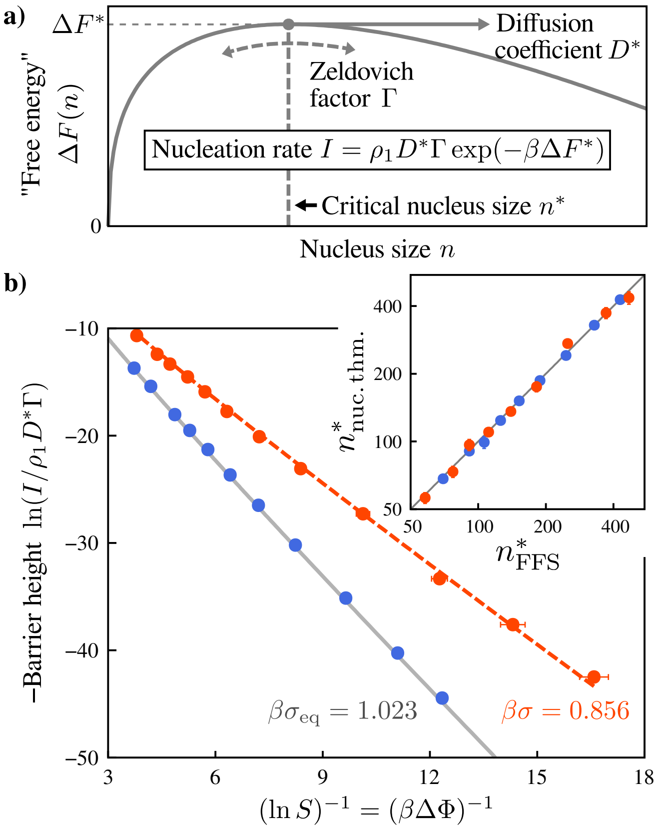

FIG. 2. **Nucleation kinetics at a NESS obey classical nucleation theory (CNT) with modified interfacial properties.** **(a)** A schematic illustration of diffusion on an (equilibrium) free-energy landscape, $F(n)$. **(b)** Tests of CNT and the nucleation theorem (inset) for nonequilibrium homogeneous (blue) and inhomogeneous (orange) models under far-from-equilibrium conditions (at $\beta\Delta\mu_{\mathrm{coex}} = 1.87$ using the same parameters as Fig. 1c,d). Solid and dashed curves show the equilibrium prediction and a fit of the inhomogeneous results to the CNT rate equation, respectively.

a minimum free-energy pathway along a reaction coordinate corresponding to the size of a nucleus of the stable phase. This pathway crosses a free-energy barrier that arises from the competition between the lower thermodynamic potential of the stable phase and the positive interfacial free energy between the nucleus and the bulk metastable phase. CNT predicts that the homogeneous nucleation rate density is the product of a prefactor and a Boltzmann factor corresponding to the height of the barrier, ΔF^*; the prefactor is the product of the monomer number density, ρ_1; the speed along the reaction coordinate at the top of the barrier, D^*; and the Zeldovich factor, Γ, that accounts for fluctuations that cross the barrier but return to the metastable state (Fig. 2a). After taking into account the interfacial free energy due to the macroscopic line tension and microscopic nucleus size fluctuations, CNT has been shown to provide a quantitative description of nucleation in the two-dimensional equilibrium lattice gas model [28].

We employ forward-flux sampling (FFS) [29] to compute the nucleation rate density, I, and the commitment probability to the stable phase, $\phi(n)$, using the largest nucleus size, n, as the reaction coordinate. The critical nucleus size, n^*, is found where $\phi(n^*) = 1/2$ [30], and the Zeldovich factor can be calculated by fitting $\phi(n)$ to an approximately harmonic barrier in the vicinity of n^*. We also independently measure the number density of bonding-state monomers in the vapor phase, ρ_1, and the diffusion coefficient, D^*, from nucleus-size fluctuations near n^* [31]. We are therefore able to isolate the factor in the CNT rate equation that pertains to the (nonequilibrium) nucleation barrier by computing $\ln(I/\rho_1 D^* \Gamma)$ as a function of the supersaturation, $S \equiv \exp(\beta\Delta\Phi)$, which we control by tuning $\Delta\mu$ (Appendix B).

We first test the prediction of the fundamental nucleation theorem, $n^* = -\partial \ln(I/\rho_1 D^* \Gamma)/\partial \ln S + 1$, for nucleating a stable liquid phase from a supersaturated vapor phase [12]. This prediction holds as long as the interfacial free energy is independent of the supersaturation, regardless of the functional form of the nucleation barrier. The results of representative simulations shown in the inset of Fig. 2b demonstrate excellent agreement between the critical nucleus sizes obtained from FFS, n^*_{FFS}, and the sizes inferred from this theorem, $n^*_{\mathrm{nuc.\,thm.}}$. This provides evidence that the fundamental premise of CNT—namely, that the rate-limiting step coincides with the formation of a critical nucleus of the stable bulk phase—applies to nucleation at a NESS in the regime $\beta\Delta\Phi \lesssim 1$.

However, when examining the supersaturation dependence of the apparent nucleation barrier (Fig. 2b), we discover a surprising deviation from the equilibrium lattice gas: Although the interfacial contribution still scales with the perimeter of the two-dimensional nucleus, the inferred line tension, σ, differs from the equilibrium value, σ_{eq}. This deviation only occurs in the case of inhomogeneous reactions, which can be seen by comparing the homogeneous and inhomogeneous results with the equilibrium barrier height in Fig. 2b. These observations indicate that CNT can be extended to describe phase separation at a NESS, but that the nucleation rate can differ by orders of magnitude from predictions based on equilibrium interfacial properties in the case of nonequilibrium inhomogeneous reactions.

Our simulations reveal that the liquid–vapor interfacial properties are influenced by how far the system is driven out of equilibrium. To illustrate this effect, we perform simulations corresponding to an isothermal experiment in which the total number of particles is conserved, such that $\beta\epsilon$ and ρ_{v} are held constant. We find that the line tension for inhomogeneous reactions deviates farther from the equilibrium value as we increase $\beta\Delta\mu$ at coexistence (Fig. 3a). We also find that the interfacial properties depend on the relative timescale, k°, between $\mathrm{I} \rightleftharpoons \mathrm{B}$ transitions and the rate of particle attachment to the nucleus, normalized by its perimeter. To test the sensitivity of the line tension to the ratio of these timescales, we calculate the line tension deviation,

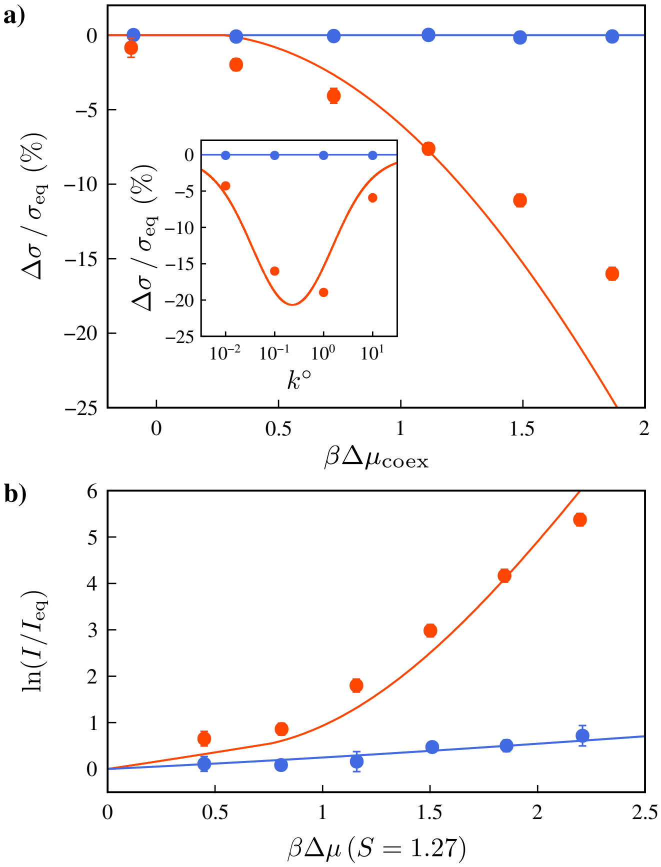

FIG. 3. **Inhomogeneous reactions at a NESS alter the interfacial tension, which strongly affects the nucleation kinetics.** **(a)** Deviation of the nonequilibrium line tension, $\Delta\sigma \equiv \sigma - \sigma_{\rm eq}$, as determined from nucleation rate calculations, with respect to $\beta\Delta\mu_{\rm coex}$ and k° (inset). The simulation parameters are the same as in Fig. 1c,d. **(b)** Comparison of nonequilibrium nucleation rates, I, to corresponding equilibrium rates, $I_{\rm eq}$, at constant supersaturation, $S = 1.27$ (see text). Orange and blue colors indicate nonequilibrium inhomogeneous and homogeneous models, respectively. Symbols report FFS results, and lines show theoretical predictions.

$\Delta\sigma$, while holding $\Delta f_{\rm res} + \Delta\mu$ constant (inset of Fig. 3a). We find that $\Delta\sigma$ is nonzero over a wide range of k°, with the greatest deviation occurring when these timescales are comparable ($k^\circ \approx 1$). However, we recover the equilibrium line tension in the limit of either zero reactive flux ($k^\circ \to 0$) or infinitely fast reactions ($k^\circ \to \infty$), as the system reverts either to a true equilibrium or to a NESS in which $\Delta\Delta f \to 0$, respectively.

We can understand these results by considering a theoretical model that captures the qualitative behavior of the nonequilibrium interface. We make the approximation that particle exchange between the open system and the reservoir relaxes to the steady-state distribution more quickly than the local environment around a particle changes. Within this "Fixed Local Environment approXimation" (FLEX), the steady-state number densities $\tilde\rho_{\rm I}$ and $\tilde\rho_{\rm B}$ map to an *effective* equilibrium system with fugacities $\tilde z_{\rm I}$ and $\tilde z_{\rm B}$ (Appendix C). Examining the internal free-energy difference $\beta\Delta f \equiv -\ln(\tilde z_{\rm B}/\tilde z_{\rm I})$ within the FLEX framework shows that a common effective equilibrium describes both phases if $k_{\rm I\to B}$ is constant, corresponding to homogeneous reactions, regardless of $\Delta\mu$. Conversely, a different effective equilibrium is needed for each phase if $k_{\rm I\to B}$ depends on u, corresponding to inhomogeneous reactions.

To predict the nonequilibrium interfacial tension from FLEX, we employ a solid-on-solid model [32] of an interface at coexistence. We first find $\beta\Delta\mu_{\rm coex}$ by setting $S_{\rm FLEX} \equiv [\tilde\rho_{\rm B}/(1-\tilde\rho_{\rm B})]_{u=2\epsilon} = 1$, where the fixed local environment $u = 2\epsilon$ is assumed based on the particle–hole symmetry of the equilibrium lattice gas. We then calculate the effective energy of attaching a single bonding-state adatom to a flat interface, $\beta\tilde\epsilon \equiv \ln\left[\tilde\rho_{\rm B}/(1-\tilde\rho_{\rm B})\right]_{u=\epsilon}$, at the coexistence points $\beta\Delta\mu_{\rm coex}$ (Appendix D). Importantly, $\tilde\epsilon$ only differs from ϵ with nonequilibrium inhomogeneous reactions. Finally, we estimate the nonequilibrium line tension by evaluating an equilibrium expression for $\sigma(\beta\tilde\epsilon)$ [33] (solid curves in Fig. 3a). In our inhomogeneous simulations, $k_{\rm I\to B}$ is a decreasing function of u, leading to a lower Δf and thus a higher population of bonding-state particles at the interface than would be expected based on the effective equilibrium model of the bulk liquid phase. This enrichment of bonding-state particles at the interface relative to the liquid phase reduces the effective adatom bonding energy in our theory, such that $|\tilde\epsilon| \leq |\epsilon|$, and lowers the effective free-energy cost of the interface.

Our key insight from this theory is that nonequilibrium interfacial properties emerge when the bulk phases and the liquid–vapor interface are described by *different* effective equilibrium models. Consequently, when $\tilde\epsilon \neq \epsilon$, bonding particles attached to the interface of a critical nucleus may be attracted either more or less strongly, per nearest-neighbor interaction, than in the bulk liquid phase. Our theory captures both the sign and the approximate functional form of $\Delta\sigma$ with respect to $\beta\Delta\mu_{\rm coex}$, as well as the nonmonotonic dependence of $\Delta\sigma$ on the relative reaction timescale k°. While the precise form of $\Delta\sigma$ depends on our choice of simulation parameters, the generality of our theory suggests that a nonzero $\Delta\sigma$ can arise whenever the effective internal free-energy difference is a function of the local environment.

Finally, to highlight the control over nucleation rates imparted by inhomogeneous reactions, we compare the nonequilibrium nucleation rate to that of an equilibrium fluid with the same $\beta\epsilon$, S, and $\rho_{\rm v}$ (Fig. 3b). In agreement with our theory, our simulations show that the nucleation rate can be increased by orders of magnitude relative to the corresponding equilibrium system by driving the fluid far from equilibrium ($\beta\Delta\mu \gg 1$). The magnitude of this effect is far greater in the inhomogeneous than in the homogeneous model due to the dominant role of the line tension in determining the nucleation barrier, and thus the nucleation rate. Inhomogeneous reactions can therefore break the usual relationship between high supersaturation and fast nucleation, offering a novel way to control nucleation kinetics in nonequilibrium fluids.

In conclusion, we have introduced a strategy for simulating nonequilibrium phase transformations within the framework of stochastic thermodynamics. By showing that inhomogeneous chemical reactions can give rise to nonequilibrium interfacial tensions, our work reveals a mechanism for decoupling nucleation rates from thermodynamic driving forces at a NESS. Our findings provide further evidence [1, 2] that nonequilibrium phase transformations may follow the same phenomenological laws as equilibrium systems under rather general conditions. Detecting nonequilibrium effects may thus require careful measurements of interfacial material properties.

We emphasize that our qualitative results do not depend on the specific form of the reaction rates: The only essential ingredient is an inhomogeneously driven reaction that is either promoted or suppressed by variations in the local potential energy. For example, if the reactive flux through the driven pathway is enhanced at low potential energies, as in our simulations, then our model can describe either preferentially driven deactivation (B → I) in the liquid phase or preferentially driven activation (I → B) in the vapor phase. The former scenario represents an implicit description of enzyme-mediated deactivation, in which the chemical fuel is uniformly distributed but the enzymes that catalyze B → I reactions preferentially partition into the condensed, low-potential-energy phase. Such a scenario has been proposed to describe inhomogeneous enzyme distributions associated with stress granules and other biological condensates [3, 34, 35].

Our results are applicable to a range of experimental systems broadly described as living or active. Our prediction of a nonequilibrium surface tension could be tested in the context of intracellular condensates using light-activated corelets [36], which have recently been applied to study condensate nucleation *in vivo* [19]. Our model could also be applied to synthetic active polypeptide coacervates [37–39] or DNA liquids [40] in which the association/hybridization reactions are engineered to respond to energy input in a manner that is dependent on the local protein/DNA concentration. In both contexts, our results suggest a road map for controlling self-assembly kinetics far from thermal equilibrium.

This work is supported by the National Science Foundation (DMR-2143670).

Appendix A: Nonequilibrium lattice-gas model

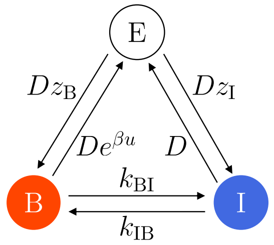

FIG. A1. **Kinetic scheme of particle exchange and internal chemical reactions.** In our simulations of an open system, each lattice site stochastically transitions between being unoccupied (E) or being occupied by either a bonding (B) or inert (I) particle with the specified transition rates.

We extend the two-dimensional square lattice-gas model by incorporating two particle internal states: a bonding state (B) and an inert state (I). B-state particles interact with nearest-neighbor B-state particles with bonding strength $\epsilon < 0$. By contrast, I-state particles are isoenergetic to empty lattice sites and thus do not interact with nearest-neighbor particles. Here we consider an open system in contact with a particle reservoir, such that B and I-state particles have fugacities $z_{\rm B}$ and $z_{\rm I}$, respectively, in the reservoir. Open systems have similar advantages for studying nonequilibrium phase transitions as the grand-canonical ensemble does for equilibrium systems, including the elimination of interfaces and a resulting reduction of finite size effects [24].

Utilizing the framework of stochastic thermodynamics, we model the kinetics of particle insertion, removal, and reactions between internal states using Markovian transitions that obey local detailed balance [20, 21]. Particle insertion and removal rates depend on the reservoir fugacities, $z_{\rm B}$ and $z_{\rm I}$; the local potential energy u due to nearest-neighbor interactions at a particular lattice site; and the base exchange rate, D, between the open system and the reservoir (Fig. A1). Reactions between the B and I states occur with forward and backward rates $k_{\rm BI}$ and $k_{\rm IB}$. We introduce dimensionless ratios between tje reaction and particle-exchange rates, $k_{\rm B\to I} \equiv D^{-1}k_{\rm BI}$ and $k_{\rm I\to B} \equiv D^{-1}k_{\rm IB}$, for notational simplicity. We simulate the stochastic evolution of the system via the kinetic Monte Carlo method [23].

We define the nonequilibrium drive $\Delta\mu$ along the single-cycle network (Fig. A1) in the B-to-I direction,

$$\beta\Delta\mu = \ln\left[z_{\rm B}k_{\rm B\to I}/z_{\rm I}k_{\rm I\to B}e^{\beta u}\right]. \tag{A1}$$

Time-reversal symmetry is broken when the system is driven out-of-equilibrium ($\Delta\mu \neq 0$), resulting in a nonzero net probability current. Rearranging Eq. (A1) gives the local detailed balance condition for I $\rightleftharpoons$ B reactions in terms of the chemical drive $\Delta\mu$,

$$k_{\rm B\to I}/k_{\rm I\to B} = \exp(\beta u + \beta\Delta f_{\rm res} + \beta\Delta\mu), \tag{A2}$$

where $\beta\Delta f_{\rm res} \equiv -\ln(z_{\rm B}/z_{\rm I})$ is the internal free-energy difference in the reservoir.

In our simulations, we consider two specific choices for the backward reaction rate, $k_{\rm I\to B}$, in order to model homogeneous and inhomogeneous chemical reactions. For *homogeneous* systems, we set $k_{\rm I\to B}$ equal to a constant k° representing the ratio between the timescales for chemical reactions and particle transport. For *inhomogeneous* systems, we assume that $k_{\rm I\to B}$ is u-dependent and takes a Metropolis form, $k_{\rm I\to B} = k^\circ \min[1, \exp(-\beta u - \beta\Delta f_{\rm res} - \beta\Delta\mu)]$. Note that $k_{\rm B\to I}$ follows from the local detailed balance condition, Eq. (A2), in both cases.

We quantify the extent of inhomogeneous chemical reactions by estimating the effective free-energy difference between the two particle internal states, Δf, from simulations of each bulk phase. A lattice configuration is defined by the lattice-site occupancies, $\{c(\boldsymbol{r})\}$, where $c \in \{\text{E}, \text{B}, \text{I}\}$ and $z_{\rm E} = 1$. The equilibrium probability that the tagged site at the origin, $\boldsymbol{r} = 0$, is in state i is

$$\frac{p^{\rm eq}_{i(\boldsymbol{r}=0)}}{p^{\rm eq}_{j(\boldsymbol{r}=0)}} = \left(\frac{z_i}{z_j}\right)\left\langle e^{-\beta\sum_{\boldsymbol{r}'} u[i,c(\boldsymbol{r}')] - u[j,c(\boldsymbol{r}')]}\right\rangle_{j(\boldsymbol{r}=0)}, \tag{A3}$$

where summation is over the nearest-neighbor sites $\boldsymbol{r}'$ of the tagged site, $u[i,j]$ is the potential energy between nearest-neighbor lattice sites in states i and j, and angle brackets indicate an ensemble average conditioned on the tagged site being in the indicated state. We use Eq. (A3) to define the effective Δf by substituting $p^{\rm eq}$ with the NESS distribution, p, and averaging over the NESS,

$$\beta\Delta f = -\ln\left(\frac{p_{\rm B}}{p_{\rm I}}\right) + \ln\left\langle e^{-\beta\sum_{\boldsymbol{r}'} u[\text{B},c(\boldsymbol{r}')]}\right\rangle_{\text{I}(\boldsymbol{r}=0)}. \tag{A4}$$

Appendix B: Determining the interfacial tension in nonequilibrium nucleation simulations

The free-energy landscape along the nucleus-size reaction coordinate, n, in the equilibrium lattice gas is [28]

$$\beta F(n) = \beta\sigma\sqrt{4\pi n} - \beta\Delta\Phi n + {}^{5}\!/\!_{4}\ln n + d, \tag{B1}$$

where d is a constant chosen to equate the B-state monomer number density in the vapor phase, ρ_1, and $\exp[-\beta F(1)]$, such that the barrier height is $\Delta F^* \equiv F(n^*) - F(1)$. From the CNT rate density, $I = \rho_1 D^*\Gamma\exp(-\beta F^*)$, we obtain

$$\ln\left(\frac{I}{\rho_1 D^*\Gamma}\right) = \beta\Delta\Phi(n^*-1) - \beta\sigma\sqrt{4\pi}(\sqrt{n^*}-1) - {}^{5}\!/\!_{4}\ln n^*, \tag{B2}$$

where $n^* = 25/(-\beta\sigma\sqrt{4\pi} + \sqrt{4\pi\beta^2\sigma^2 + 20\beta\Delta\Phi})^2$ is the critical nucleus size, and $\ln(I/\rho_1 D^*\Gamma)$ is an approximately linear function of $1/\beta\Delta\Phi$ with slope proportional to $-\sigma^2$ (Fig. 2b). Using FFS simulations on a 64×64 lattice, we measure ρ_1 in the vapor phase and calculate D^* by analyzing the diffusive behavior of the reaction coordinate when $n \approx n^*$. The Zeldovich factor, Γ, is found independently by fitting the commitment probabilities, $\phi(n)$, calculated in FFS simulations,

$$\phi(n) \approx \frac{1}{2}\mathrm{erf}\left[\Gamma\sqrt{\pi}(n-n^*)\right] + \frac{1}{2}, \tag{B3}$$

where erf is the error function, and we have assumed that the landscape is approximately parabolic near $n \approx n^*$. We obtain the line tension, σ, by fitting Eq. (B2) over a range of $\beta\Delta\Phi$ values determined from nonequilibrium umbrella sampling, using σ as the sole fitting parameter.

Appendix C: Fixed Local Environment approXimation (FLEX)

In the Fixed Local Environment approXimation (FLEX), we assume that particle exchange between the open system and the reservoir relaxes to the steady state more rapidly than any change in the local configuration, or environment, around a tagged lattice site. Specifically, we represent the configuration around a tagged lattice site by a fixed number of nearest-neighbor B-state particles (Fig. A2). We then calculate the single-site steady-state distribution, $\tilde{\rho}_i$, from the Markovian transition network shown in Fig. A1; $\tilde{\rho}_i$ may be regarded as the number density of a particle, if $i = \mathrm{B}$ or I, or a vacancy, if $i = \mathrm{E}$.

We map our nonequilibrium model to an *effective* equilibrium that has the same steady-state distribution $\tilde{\rho}$ as that predicted by FLEX. To this end, we define effective fugacities in the open system, $\tilde{z}_\mathrm{B} \equiv (\tilde{\rho}_\mathrm{B}/\tilde{\rho}_\mathrm{E})\exp(\beta u)$ and $\tilde{z}_\mathrm{I} \equiv \tilde{\rho}_\mathrm{I}/\tilde{\rho}_\mathrm{E}$, and the single-site partition function $\tilde{\xi} = 1 + \tilde{z}_\mathrm{B} + \tilde{z}_\mathrm{I}$. Depending on the functional form of $k_{\mathrm{I}\to\mathrm{B}}$, the effective fugacities may depend on u, and the liquid and vapor phases may be mapped to different effective equilibrium models. We therefore calculate the effective internal free-energy difference, Δf, between the B and I states in the open system, as in Eq. (A4). Within FLEX, $\beta\Delta f \equiv -\ln(\tilde{z}_\mathrm{B}/\tilde{z}_\mathrm{I})$ is related to $\beta\Delta f_\mathrm{res}$ by

$$\beta\Delta f = \beta\Delta f_\mathrm{res} + \ln\left[\frac{1 + k_{\mathrm{I}\to\mathrm{B}}(1 + e^{\beta\Delta f_\mathrm{res}})e^{\beta\Delta\mu}}{1 + k_{\mathrm{I}\to\mathrm{B}}(1 + e^{\beta\Delta f_\mathrm{res}})}\right]. \tag{C1}$$

Eq. (C1) predicts the requirements for coexisting phases, which have different average potential energies per lattice site, to be thermodynamically inhomogeneous: For Δf to be u-dependent, $k_{\mathrm{I}\to\mathrm{B}}$ must be u-dependent and chemical drive must be applied ($\Delta\mu \neq 0$). These conditions are consistent with the simulation results shown in Fig. 1d.

Appendix D: FLEX prediction of the nonequilibrium interfacial tension

Phase coexistence in the two-dimensional equilibrium lattice gas occurs at $\mu = 2\epsilon$, where μ is the particle chemical potential, due to particle–hole symmetry [22]. The resulting supersaturation $S \approx \exp[\beta(\mu - 2\epsilon)]$ in the equilibrium model can be interpreted as the ratio $\rho/(1-\rho)$ at a tagged lattice site with exactly two neighboring particles, where ρ is the particle number density. Assuming that particle–hole symmetry is a reasonable approximation for the effective equilibrium as well, we define the FLEX supersaturation, S_FLEX, based on the steady-state distribution at a tagged lattice site with $u = 2\epsilon$,

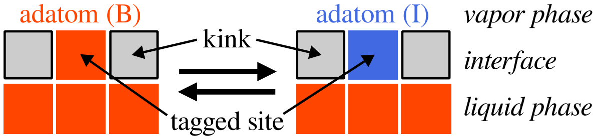

FIG. A2. **FLEX schematic of a single-layer configuration at a liquid–vapor interface.** The effective bonding energy at the interface is obtained from the steady-state distribution at the tagged site under a fixed local configuration. Colors correspond to the same lattice-site states as in Fig. A1.

$$S_\mathrm{FLEX} \equiv \left[\frac{\tilde{\rho}_\mathrm{B}}{1-\tilde{\rho}_\mathrm{B}}\right]_{u=2\epsilon} = \frac{\tilde{z}_\mathrm{B}(2\epsilon;\Delta\mu)e^{-2\beta\epsilon}}{1 + \tilde{z}_\mathrm{I}(2\epsilon;\Delta\mu)}. \tag{D1}$$

We then predict the NESS coexistence point by solving for the chemical drive at which $S_\mathrm{FLEX} = 1$, subject to an imposed total particle density in the vapor phase.

We use FLEX to predict the interfacial tension by considering the attachment of a single bonding-state particle to a flat liquid–vapor interface in a solid-on-solid model at phase coexistence. We focus on the effective bonding energy $\beta\tilde{\epsilon}$ of a single adatom, since the coexistence condition $S_\mathrm{FLEX} = 1$ implies that the formation of a kink on the interface (Fig. A2) incurs no (effective) free-energy cost. To determine $\beta\tilde{\epsilon}$, we apply FLEX to a tagged adatom site with $u = \epsilon$ at the predicted coexistence point, $\Delta\mu_\mathrm{coex}$. Because the equilibrium free-energy cost to attach an adatom to a flat interface is $\beta\epsilon$, we define the effective bonding energy $\beta\tilde{\epsilon}$ in the same way:

$$\beta\tilde{\epsilon} \equiv \ln\left[\frac{\tilde{\rho}_\mathrm{B}}{1-\tilde{\rho}_\mathrm{B}}\right]_{u=\epsilon} = \ln\left[\frac{\tilde{z}_\mathrm{B}(\epsilon;\Delta\mu_\mathrm{coex})}{1+\tilde{z}_\mathrm{I}(\epsilon;\Delta\mu_\mathrm{coex})}\right] - \beta\epsilon. \tag{D2}$$

In homogeneous systems, this prediction reduces to $\beta\tilde{\epsilon} = \beta\epsilon$, meaning that the effective adatom interaction strength does not change no matter how far the system is driven out of equilibrium. However, in the case of inhomogeneous chemical reactions, $\beta\tilde{\epsilon}$ may differ from $\beta\epsilon$.

Finally, we predict the nonequilibrium interfacial tension, σ, using the adatom interaction strength $\beta\tilde{\epsilon}$ at the interface and the equilibrium formula [33]

$$\sigma(\tilde{\epsilon}) = \sqrt{\frac{4\tilde{\epsilon}\beta^{-2}}{\pi\chi(\beta)}\int_{\beta_c}^{\beta} K'\left(\frac{8[\cosh(\beta'\tilde{\epsilon})-1]}{[\cosh(\beta'\tilde{\epsilon})+1]^2}\right)\left[\frac{\cosh(\beta'\tilde{\epsilon})-3}{\sinh(\beta'\tilde{\epsilon})}\right]d\beta'}, \tag{D3}$$

where K' is the elliptic integral of the first kind, $\chi(\beta) = [1 - \sinh^{-4}(\beta\tilde{\epsilon}/2)]^{1/8}$, and β_c is the inverse critical temperature given by $\beta_\mathrm{c}|\tilde{\epsilon}| = 2\ln(1+\sqrt{2})$. We find that this FLEX prediction qualitatively explains the decreasing trend of the line tension with respect to the nonequilibrium drive in the inhomogeneous model (see Fig. 3a).

[1] J. Berry, C. P. Brangwynne, and M. Haataja, Rep. Prog. Phys. **81**, 046601 (2018).

[2] C. A. Weber, D. Zwicker, F. Jülicher, and C. F. Lee, Rep. Prog. Phys. **82**, 064601 (2019).

[3] J. Söding, D. Zwicker, S. Sohrabi-Jahromi, M. Boehning, and J. Kirschbaum, Trends Cell Biol. **30**, 4 (2020).

[4] G. Bartolucci, O. Adame-Arana, X. Zhao, and C. A. Weber, Biophys. J. **120**, 4682 (2021).

[5] J. Kirschbaum and D. Zwicker, J. R. Soc. Interface **18**, 20210255 (2021).

[6] D. Zwicker, Curr. Opin. Colloid Interface Sci. **61**, 101606 (2022).

[7] D. Zwicker, A. A. Hyman, and F. Jülicher, Phys. Rev. E **92**, 012317 (2015).

[8] D. Zwicker, R. Seyboldt, C. A. Weber, A. A. Hyman, and F. Jülicher, Nature Phys. **13**, 408 (2017).

[9] J. D. Wurtz and C. F. Lee, Phys. Rev. Lett. **120**, 078102 (2018).

[10] Y. I. Li and M. E. Cates, J. Stat. Mech.: Theory Exp. , (2020) 053206.

[11] D. W. Oxtoby, J. Phys.: Condens. Matter **4**, 7627 (1992).

[12] R. P. Sear, J. Phys.: Condens. Matter **19**, 033101 (2007).

[13] S. Whitelam and R. L. Jack, Annu. Rev. Phys. Chem. **66**, 143 (2015).

[14] J. D. Perlmutter and M. F. Hagan, Annu. Rev. Phys. Chem. **66**, 217 (2015).

[15] W. B. Rogers, W. M. Shih, and V. N. Manoharan, Nat. Rev. Mater. **1**, 16008 (2016).

[16] W. M. Jacobs and D. Frenkel, J. Am. Chem. Soc. **138**, 2457 (2016).

[17] A. Hensley, W. M. Jacobs, and W. B. Rogers, Proc. Natl. Acad. Sci. U.S.A. **119**, e2114050118 (2022).

[18] Y. Shin and C. P. Brangwynne, Science **357**, eaaf4382 (2017).

[19] S. F. Shimobayashi, P. Ronceray, D. W. Sanders, M. P. Haataja, and C. P. Brangwynne, Nature **599**, 503 (2021).

[20] U. Seifert, Rep. Prog. Phys. **75**, 126001 (2012).

[21] C. Van den Broeck and M. Esposito, Physica A **418**, 6 (2015).

[22] R. K. Pathria, *Statistical mechanics*, 2nd ed. (Butterworth-Heinemann, Oxford, 1996).

[23] D. T. Gillespie, Annu. Rev. Phys. Chem **58**, 35 (2007).

[24] N. B. Wilding, Phys. Rev. E **52**, 602 (1995).

[25] A. Warmflash, P. Bhimalapuram, and A. R. Dinner, J. Chem. Phys. **127**, 154112 (2007).

[26] See Supplementary Material [URL will be inserted by the publisher] for a detailed description, which includes [41] and [42].

[27] D. Chandler, *Introduction to modern statistical mechanics* (Oxford University Press, New York, 1987).

[28] S. Ryu and W. Cai, Phys. Rev. E **81**, 030601 (2010).

[29] R. J. Allen, C. Valeriani, and P. R. ten Wolde, J. Phys.: Condens. Matter **21**, 463102 (2009).

[30] G. Hummer, J. Chem. Phys. **120**, 516 (2004).

[31] S. Auer and D. Frenkel, Annu. Rev. Phys. Chem. **55**, 333 (2004).

[32] Y. Saito, *Statistical physics of crystal growth* (World Scientific, Singapore, 1996).

[33] V. A. Shneidman, K. A. Jackson, and K. M. Beatty, J. Chem. Phys. **111**, 6932 (1999).

[34] M. Hondele, S. Heinrich, P. De Los Rios, and K. Weis, Emerg. Top. Life Sci. **4**, 343 (2020).

[35] B. G. O'Flynn and T. Mittag, Curr. Opin. Cell Biol. **69**, 70 (2021).

[36] D. Bracha, M. T. Walls, M.-T. Wei, L. Zhu, M. Kurian, J. L. Avalos, J. E. Toettcher, and C. P. Brangwynne, Cell **175**, 1467 (2018).

[37] K. K. Nakashima, J. F. Baaij, and E. Spruijt, Soft Matter **14**, 361 (2018).

[38] F. Späth, C. Donau, A. M. Bergmann, M. Kränzlein, C. V. Synatschke, B. Rieger, and J. Boekhoven, J. Am. Chem. Soc. **143**, 4782 (2021).

[39] K. K. Nakashima, M. H. van Haren, A. A. M. André, I. Robu, and E. Spruijt, Nat. Commun. **12**, 3819 (2021).

[40] O. A. Saleh, B.-j. Jeon, and T. Liedl, Proc. Natl. Acad. Sci. U.S.A. **117**, 16160 (2020).

[41] E. G. Noya, C. Vega, and E. de Miguel, J. Chem. Phys. **128**, 154507 (2008).

[42] J.-P. Hansen and I. R. McDonald, *Theory of simple liquids: with applications to soft matter*, 4th ed. (Academic press, Oxford, 2013).